Ultra-Stable N-Type Semiconducting Fiber Organic Electrochemical Transistors for Highly Sensitive Biosensors

Xiu Wang, Zhi Zhang, Peiyun Li, Jingcao Xu, Yuting Zheng, Wenxi Sun, Mingyue Xie, Juanrong Wang, Xiran Pan, Xun Lei, Jingyi Wang, Jupeng Chen, Yiheng Chen, Shu-Jen Wang, Ting Lei**

X. Wang, Z. Zhang, P. Li, J. Xu, W. Sun, M. Xie, J. Wang, X. Pan, X. Lei, J. Wang, J. Chen, Y. Chen, T. Lei

Key Laboratory of Polymer Chemistry and Physics of Ministry of Education

School of Materials Science and Engineering

Peking University

100871, Beijing, P. R. China

E-mail: zhizhang@pku.edu.cn (Zhi Zhang); tinglei@pku.edu.cn (Ting Lei)

Y. Zheng,

College of Engineering

This article has been accepted for publication and undergone full peer review but has not been through the copyediting, typesetting, pagination and proofreading process, which may lead to differences between this version and the Version of Record. Please cite this article as doi: 10.1002/adma.202400287.

Peking University

100871, Beijing, P. R. China

S.-J. Wang

Department of Physics

Hong Kong Baptist University

Hong Kong SAR, P. R. China

Keywords: organic electrochemical transistors, n-type conjugated polymers, semiconducting fibers, biosensors, fiber logic circuits

Abstract: Organic electrochemical transistors (OECTs) have attracted increasing attention due to their merits of high transconductance, low operating voltage, and good biocompatibility, ideal for biosensors. However, further advances in their practical applications face challenges of low n-type performance and poor stability. Here, we demonstrate that wet-spinning the commercially available n-type conjugated polymer poly(benzimidazobenzophenanthroline) (BBL) into highly aligned and crystalline fibers enhances both OECT performance and stability. Although BBL is only soluble in high-boiling-point strong acids, it can be wet-spun into high-quality fibers with adjustable diameters. Our BBL fiber OECTs exhibit a record-high area-normalized transconductance

($g_{m,A}$) of 2.40 μS μm^{-2} and over 10 times higher figure-of-merit (μC^*) than its thin-film counterparts. More importantly, these fiber OECTs exhibit remarkable stability with no noticeable performance attenuation after 1500 cycles over 4 h operation, outperforming all previously reported n-type OECTs. The superior performance and stability can be attributed to shorter π-π stacking distance and ordered molecular arrangement in the fibers, endowing the BBL fiber OECT-based biosensors with outstanding sensitivity while keeping a miniaturized form factor. Our work demonstrates that, beyond new material development, developing new fabrication technology is also crucial for addressing the performance and stability issues in n-type OECTs.

1. Introduction

Transistor-based sensors have many advantages, such as high sensitivity, rapid response, and feasibility for miniaturization, making them promising for disease detection and health monitoring.[1-3] Transconductance (g_m), defined as the derivative of the drain current to the gate voltage ($g_m = \partial I_D/\partial V_G$), is a critical parameter for sensing, as it reflects the amplification capability and, ultimately, the sensitivity.[4-6] Enlarging the active area (the channel width (W) × length (L)) is a common strategy to enhance g_m.[5,7-9] However, a large size is undesirable for many biosensors, especially for in vivo sensing where a small size is essential to minimize tissue damage.[10-12] Specifically, neural recording demands miniaturized electronics, such as a flexible brain-machine interface typically with dimensions around or smaller than 20 × 20 μm.[13] Therefore, the active area's size is as crucial as g_m in determining device performance. Consequently, area-normalized transconductance ($g_{m,A} = g_m/WL$), which takes both g_m and

channel area into account becomes a more comprehensive metric for evaluating the performance of a transistor-based biosensor.[14]

Among various transistor-based technologies, organic electrochemical transistors (OECTs), utilizing organic semiconductors as the channel, have attracted increasing attention due to their merits of high g_m, low operating voltage, and good bio-interfacing properties.[6,15,16] However, $g_{m,A}$ was seldom considered in this OECT, which is critical for in vivo biosensing applications. Furthermore, n-type OECTs lag far behind their p-type counterparts in both performance and stability, restricting their applications in complementary logic circuits and biosensors.[17] To address these challenges, extensive efforts have been devoted to synthesizing new n-type OECT materials.[18,19] For example, many n-type OECT polymers have been developed based on high-performance building blocks, such as naphthalene diimide (NDI),[20] diketopyrrolopyrrole (DPP),[21] isoindigo (IID),[22] and bithiophene imide (BTI).[23] These efforts have significantly improved the device performance with figure-of-merits (μC^*) over 100 F cm^{-1} V^{-1} s^{-1}, approaching the state-of-the-art p-type materials. However, these new building blocks require complicated synthetic steps and high cost, with most of them not yet being commercially available. More importantly, the operational stability of the n-type OECTs remains poor, posing a great challenge to their practical applications. Therefore, a question remains: is there any simple but general approach to improving the OECT device performance and stability for biosensing?

Herein, we report that the conventional wet-spinning method can produce semiconducting fibers with enhanced performance and outstanding stability, which has not been observed before. Unlike commonly used materials design approaches, we creatively

enhanced the device performance and stability simultaneously by developing new process techniques. We selected a commercially available polymer, poly(benzimidazobenzophenanthroline) (BBL), for this study. The rapid removal of BBL solvent (methanesulfonic acid, MSA) during spinning allowed for the readily adjustment of fiber diameters while achieving high polymer chain alignment and crystallinity (**Figure 1**a-c). The BBL fiber OECTs exhibited a record-high $g_{m,A}$ of 2.40 μS μm^{-2} with over 10 times higher μC^* than its thin-film counterparts. Notably, the $g_{m,A}$ of BBL fiber OECTs is about 200 times greater than that of the reported BBL film-based ones.[24] The BBL fiber showed longer coherence length, shorter π-π stacking distance, and maintained good molecular packing along the fiber, leading to enhanced electron mobility and stability. These BBL fiber OECTs showed negligible current degradation after 1500 on-off switching cycles over 4 h operation, surpassing its thin-film devices and all other n-type OECTs. When used as biosensors, the device showed high sensitivity and good selectivity. Moreover, when paired with another p-type fiber, fiber-based complementary inverters were successfully demonstrated, exhibiting high voltage gains.

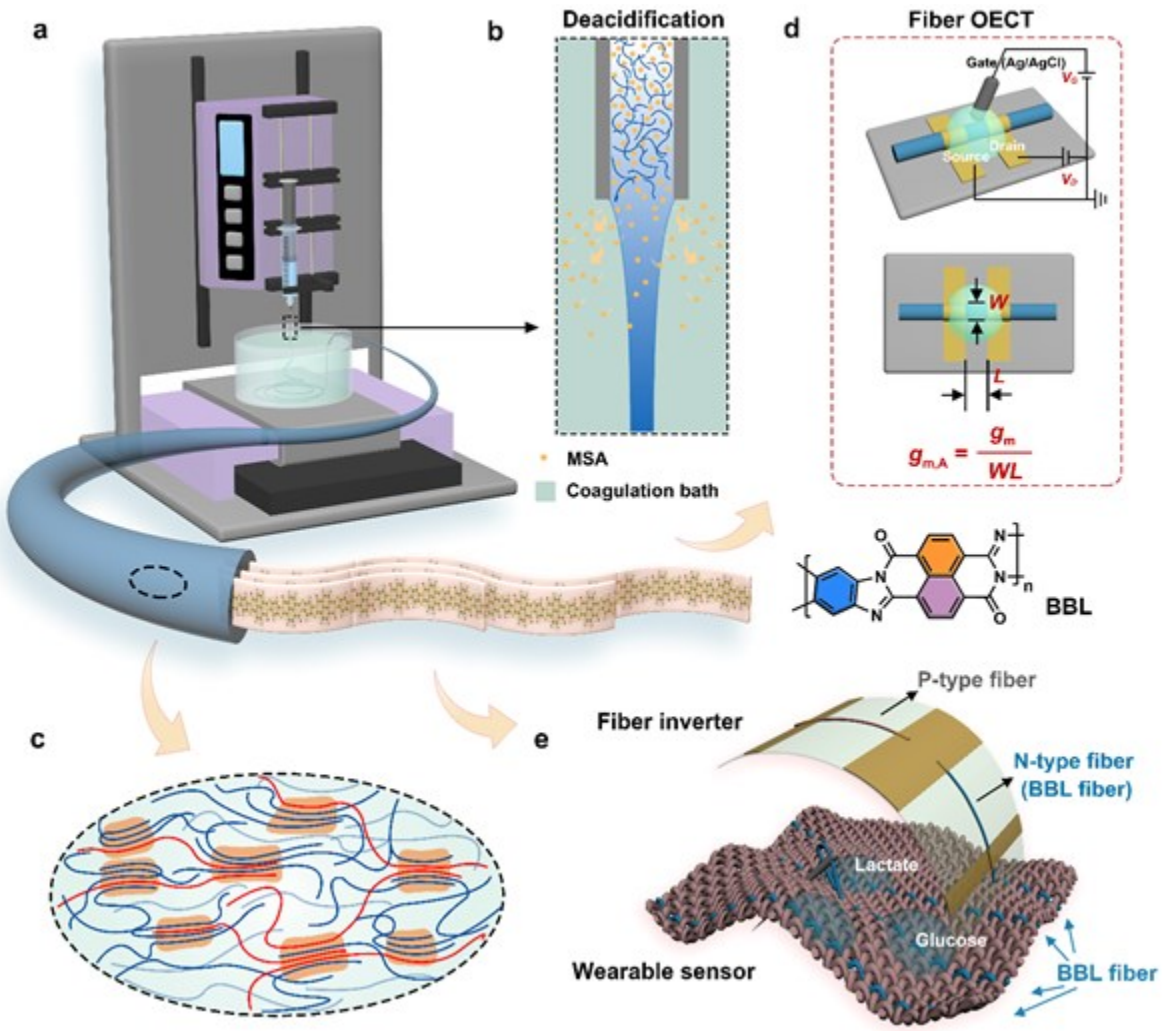

Figure 1. Schematic illustration of the fabrication and applications of BBL fibers. a) Schematic diagram of the wet-spinning system for the fabrication of BBL fibers. **b)** Deacidification of MSA in the coagulation bath during spinning. **c)** BBL molecular chain arrangements in fibers. **d)** Device configuration of the BBL fiber-based OECT. **e)** Schematic diagram of the applications of BBL fibers in complementary inverters and wearable sensors.

2. Results and Discussion

BBL is a classical n-type ladder-conjugated polymer with highly planar and rigid backbones.[25] Its side-chain-free nature makes BBL only soluble in high-boiling-point strong acids, like MSA,[26] introducing processing challenges, especially in fabricating thick BBL films. Here, commercially available BBL (Sigma-Aldrich, 667846) was utilized, and BBL microfibers were fabricated using a custom-made wet-spinning apparatus (**Figure 1**a). The rapid removal of MSA during the spinning process facilitated the convenient preparation of BBL fibers with adjustable diameters (Figure 1b). Determination of the optimal wet-spinning conditions is critical to producing BBL fibers with good mechanical and electrical properties. Fiber quality depends significantly on the spinning formulation and an appropriate coagulation bath. BBL solution with concentrations below 10 mg mL^{-1} had insufficient solid content, while concentrations exceeding 15 mg mL^{-1} were too viscous, both of which failed to facilitate fiber productions. Consequently, BBL dissolved in MSA at 10 mg mL^{-1} after filtering was used as the spinning dope.

The coagulation bath, containing an antisolvent for the polymer, plays a critical role in triggering polymer precipitation and fiber formation, further controlling the polymer chain alignment and crystallinity of fibers. Spinning needles with different diameters (*D*) and lengths (*L*') were used to regulate fiber diameter and performance. For example, the BBL fiber fabricated using a needle with *D* of 170 μm and *L*' of 38 mm was denoted as $BBL_{170,38}$ fiber. We first used a specific needle (*D*170, *L*'38) to explore the impact of the coagulation bath. We observed that BBL exhibited different spinnability in various coagulation baths, among which tetrahydrofuran (THF) and deionized (DI) water were effective for fiber formation (Figure S1, Supporting Information). Specifically, fibers formed in DI water

showed optimal uniformity, while those in THF displayed inhomogeneous morphology. Further exploration indicated that the fibers could maintain a uniform shape in a mixture of DI water and THF, as long as the THF volume remained below 30%. To optimize both the spinnability and ultimate performance of the fibers, we systematically investigated the coagulation baths with different DI water/THF ratios (Figure S2 and Table S1, Supporting Information). The microstructure of $BBL_{170,38}$ fibers obtained from different antisolvents was analyzed using wide-angle X-ray scattering (WAXS). We calculated the coherence length (L_C)[27] and para-crystalline disorder (g factor)[28] of the fibers. As the THF ratio increased in the coagulation bath, BBL fibers showed significantly increased L_C and decreased g factor (**Figure 2**a). Herman's orientation factor (f)[29] was used to quantify the chain orientation degree in the fibers, revealing enhanced f with higher THF content (Figure 2a and Table S2, Supporting Information). These results indicated that the molecular alignment and crystallinity of BBL fibers were enhanced in coagulation baths with higher THF content. Moreover, the lamellar and π-π distance decreased with the increase of THF content, indicating a more compact arrangement of BBL chains (Figure 2b).[30] Given the above, a mixture of DI water and THF with a volume ratio of 7:3 was used as the best coagulation for BBL fiber fabrication.

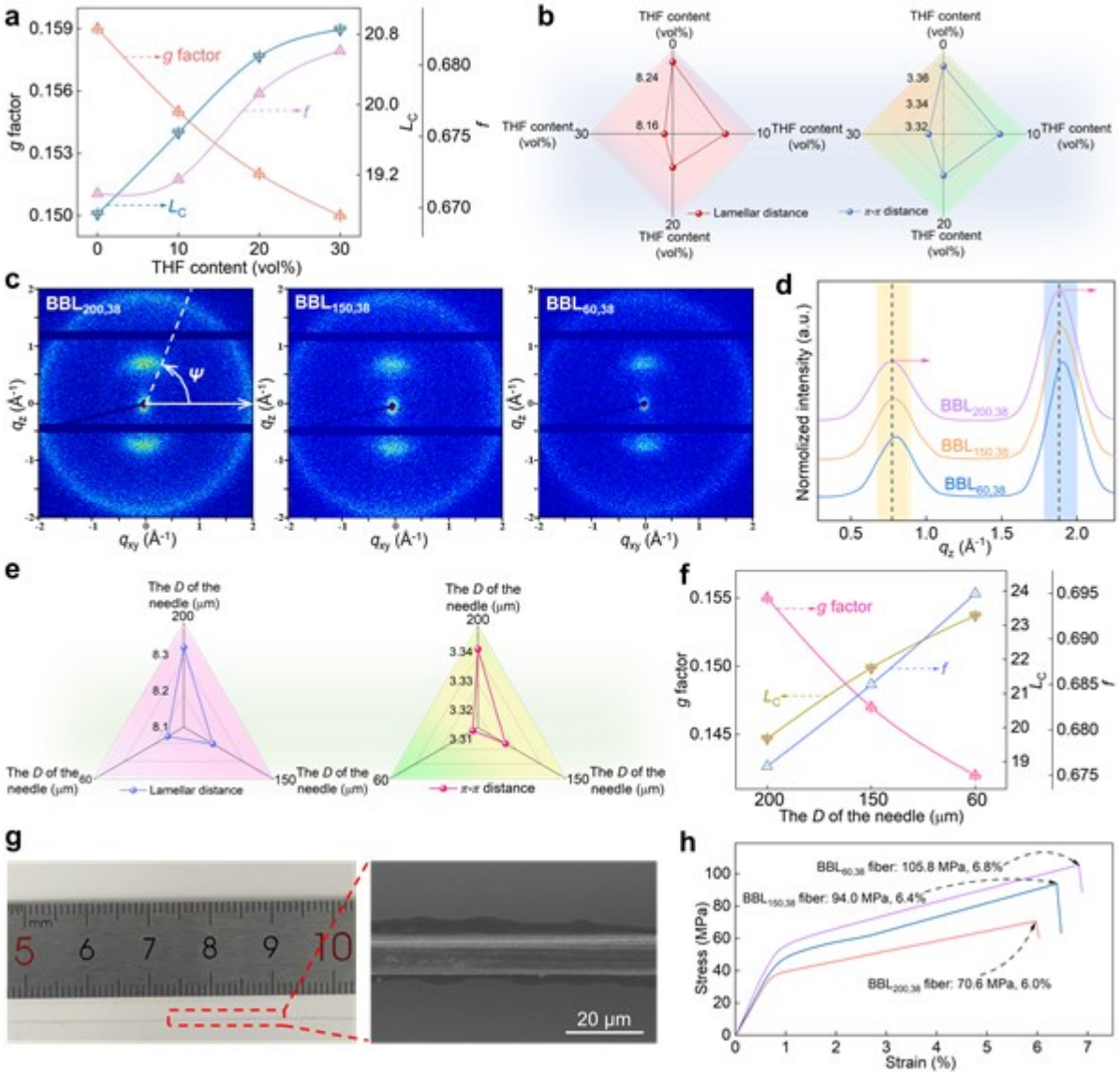

Figure 2. Fabrication, optimization, and characterization of BBL fibers. a) Comparison of the *g* factor, L_C, and *f* values of the $BBL_{170,38}$ fibers fabricated in different coagulation baths. **b)** Lamellar and π-π distance of the $BBL_{170,38}$ fibers obtained in different coagulation baths. **c)** 2D-WAXS patterns and **d)** line profiles of BBL fibers fabricated using needles with different diameters. **e)** Lamellar and π-π distance of the BBL fibers prepared using needles

with different diameters. **f)** Comparison of the *g* factor, L_C, and *f* values of BBL fibers produced using needles with different diameters. **g)** Optical photograph (left) and field-emission scanning electron microscopy (FESEM) image (right) of a typical $BBL_{60,38}$ fiber. **h)** Typical stress-strain curves of the BBL fibers with various diameters. Unless otherwise specified, a mixture of DI water and THF with a volume ratio of 7:3 was used as the coagulation bath.

The flow shear effect is also an important parameter affecting the polymer chain alignment and crystallinity, which can be tuned by adjusting the needle diameter. As the needle diameter decreased, we observed reduced lamellar and π-π distances (Figure 2c-e and Table S3, Supporting Information), enhanced L_C, reduced *g* factors, and increased chain alignment (*f* value) (Figure 2f and Table S4, Supporting Information). The closer and better molecular packing was also supported by photoluminescence (PL) spectra (Figure S6, Supporting Information). Moreover, fiber dimensions and mechanical performance are important concerns in practical applications. The fiber diameters can be adjusted by the needle size (Figure S7 and S8, Supporting Information), and $BBL_{60,38}$ fibers showed an average diameter of 10.31 ± 0.35 μm (Figure 2g), which was comparable to the size of a neuron soma,[10,31] thereby providing an inherent advantage for single-cell biosensors. Typical stress-strain curves of BBL fibers are shown in Figure 2h, where the finer fiber exhibited better mechanical strength and stretchability, achieving the highest tensile strength of 105.8 MPa and a strain-to-failure of 6.8% for the $BBL_{60,38}$ fiber. Although reducing the concentration of BBL solution could result in fibers with smaller diameters, it also led to a decrease in mechanical strength (Figure S9, Supporting Information). The tensile strength of $BBL_{60,38}$ fiber, to our knowledge, is a record-high value in semiconducting fibers and films (Figure S10 and Figure S11, Supporting Information).[32-35] Therefore, a compact and ordered

molecular arrangement in BBL fibers not only enhances mechanical strength but also contributes to improved electrical performance, a point we will demonstrate later.

BBL fibers with different dimensions coagulated in a mixture of DI water and THF (7/3, v/v) were employed as the channel materials for fiber OECT devices (Figure 1d, Figure S12, Supporting Information). All BBL fiber OECTs showed typical n-type accumulation-mode behaviors with outstanding OECT performance (**Figure 3**a,b). The normalized g_m ($g_{m,norm}$) values of the OECTs exhibited a fiber size-dependent trend (Figure S13, Supporting Information), and we calculated their μC^* values to compare their intrinsic OECT performance (Figure S14, Supporting Information).[23] Specifically, $BBL_{60,38}$ fiber OECT showed a high μC^* of 13.10 ± 0.23 F cm^{-1} V^{-1} s^{-1} (Figure 3c), which is over 10 times higher than that of the BBL film OECT (1.04 F cm^{-1} V^{-1} s^{-1}) (Figure S15, Supporting Information). The enhancement can be attributed to the improved electron mobility arising from the ordered alignment of molecular chains along the fiber direction (Figure S16, Supporting Information).[30] As discussed above, since $g_{m,A}$ is more suitable for evaluating the performance of transistor-based biosensors, we employ $g_{m,A}$ to compare the performance of different fibers. $BBL_{60,38}$ fiber OECT achieved a high $g_{m,A}$ value of 2.40 μS μm^{-2}, which surpassed that of the reported n-type film-based ones, exhibiting nearly one order of magnitude enhancement (Figure 3d). To increase g_m, film OECTs typically use thick semiconducting channels, however, this inevitably compromises μC^*.[14] It was noteworthy that our method simultaneously improved both $g_{m,A}$ and μC^*. In addition, the BBL fiber OECTs exhibited fast response speeds, enough for most biosensing applications (Figure S17, Supporting Information). We attributed the significantly improved performance to highly aligned chains and better crystallinity, as well as compacted molecular packing, which all contribute to efficient charge carrier transport along the fiber direction.

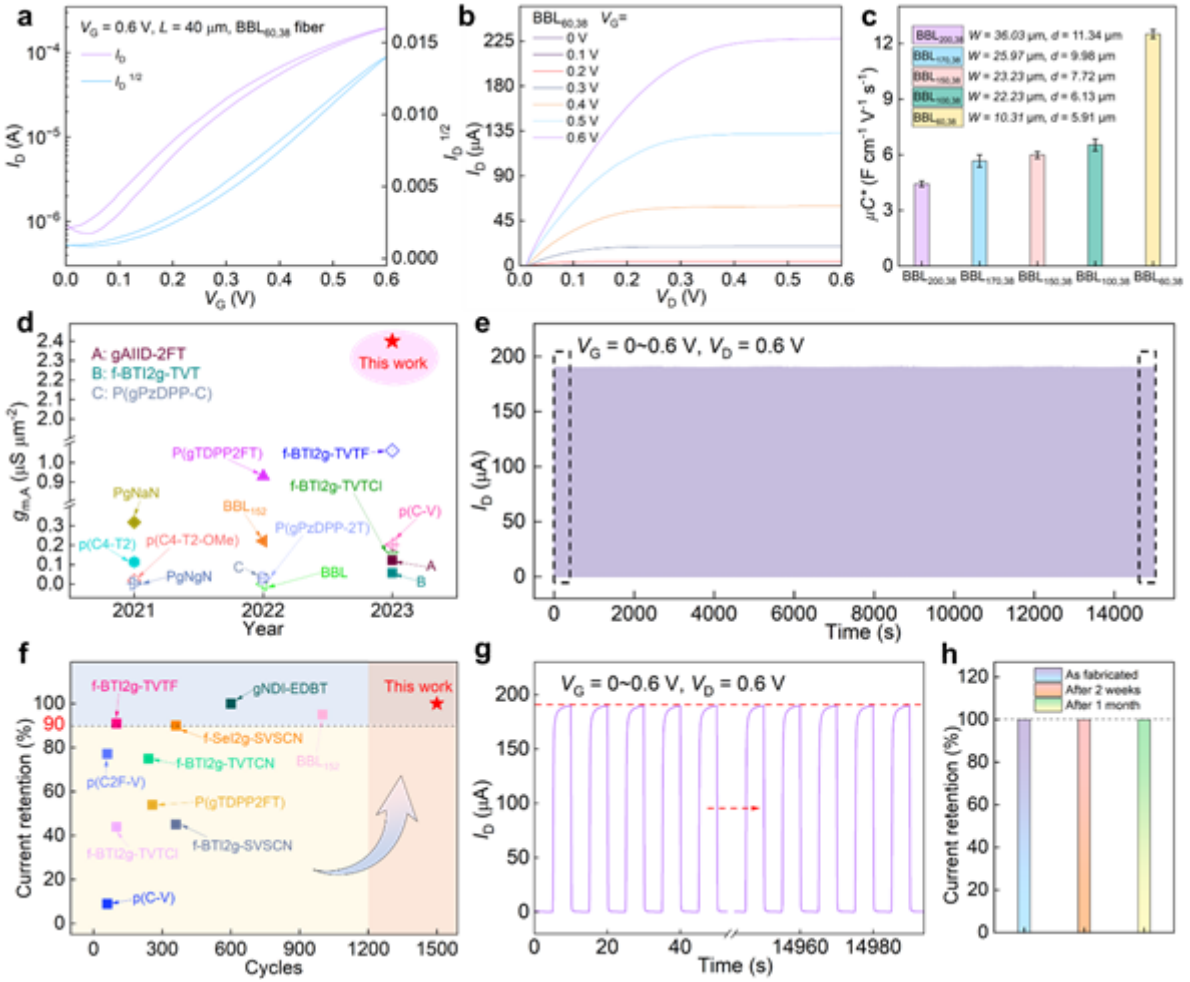

Figure 3. Fiber OECT performance and stability characterization. a) Transfer and **b)** output characteristics of $BBL_{60,38}$ fiber OECT. The channel width (W) and thickness (d) were the fiber diameter and thickness, and the channel length (L) was 40 μm. **c)** μC^* values of BBL fiber OECTs with different channel dimensions. **d**) Comparison of $g_{m,A}$ for $BBL_{60,38}$ fiber OECT and other reported n-type OECTs. **e)** Operational stability of $BBL_{60,38}$ fiber OECT under 1500 on-off cycling measurements in the air (V_G = 0~0.6 V, V_D = 0.6 V, pulse length = 10 s). **f)** Comparison of stability for $BBL_{60,38}$ fiber OECT and other reported n-type

OECTs. **g)** The enlargement of the rectangle-labeled part of e). **h)** Current retention of $BBL_{60,38}$ fiber OECT over operational time.

When used for sensors, the device's stability is crucial for reproducibility and prolonged operation. However, at present, n-type OECTs encounter challenges in achieving long-time air-stable operation, with most devices experiencing a dramatic drop in channel current (I_D) after only a few cycles, usually below 500.[23,36] Surprisingly, our $BBL_{60,38}$ fiber OECT showed excellent stability with negligible current attenuation after continuous operation over 4 h with 1500 on-off cycling measurements in the air (Figure 3e,g). Even after being kept in the air for 1 month, no visible current decline was observed, maintaining a current retention of 100% (Figure 3h and Figure S18, Supporting Information). Such high operational stability has never been achieved before (Figure 3f). Although BBL is known for its good stability, however, the reported optimal stability of the BBL OECT devices only presented a current retention of 95% after 1000 on-off switching cycles.[30] Thus, our fiber OECTs exhibited improved device stability compared to their thin-film counterparts. We performed an electrochemical quartz crystal microbalance with dissipation monitoring (EQCM-D) measurement to explore the origin of the stability (Figure S19, Supporting Information). We found that the BBL fibers showed less passive and active swelling during the electrochemical doping and dedoping process. Therefore, the better device stability can be attributed to the closer π-π stacking and enhanced polymer chain alignment in the BBL fibers, which has been proved in the WAXS (Figure 2a-f) and PL studies (Figure S6, Supporting Information).

The high $g_{m,A}$, and excellent operational stability make BBL fiber OECT a promising device for real-time, highly sensitive biosensors. We explored the fiber OECT-based sensors for potential lactate and glucose sensing. **Figure 4**a illustrates the diagram of the wearable

sensors on different substrates for lactate and glucose sensing. A modified gate electrode was used for sensing. The electrons generated during the enzymatic reaction could be directly transferred to the gate electrode, leading to a larger gate voltage (V_G) and increased I_D. Figure 4b presents the chronoamperometric response of the $BBL_{60,38}$ fiber OECT-based sensor to different concentrations of lactate in the presence of lactate oxidase (LOx) in PBS. The I_D increased with the increase of lactate concentrations with a high linear response ($R^2 = 0.9949$) within the concentration range of 10 to 200 μM, demonstrating a high sensitivity of 26.09 NR/dec (Figure 4c). The glucose sensor also exhibited a high sensitivity of 17.95 NR/dec and a good linear response (Figure 4d,e). These sensitivities remain at a record-high level compared to recently reported sensors (Figure 4f). To rule out the possibility of the active material on the gate electrode exhibiting inherent catalytic activity toward biomolecules, we tested the selectivity of the fiber glucose sensor. Figure 4g shows the I_D response by adding non-relevant biomolecules (including PBS, lactate, and fructose) and glucose solutions. The negligible responses to the non-relevant biomolecules while the remarkable response to glucose, confirmed the good selectivity of BBL fiber OECT-based sensors.

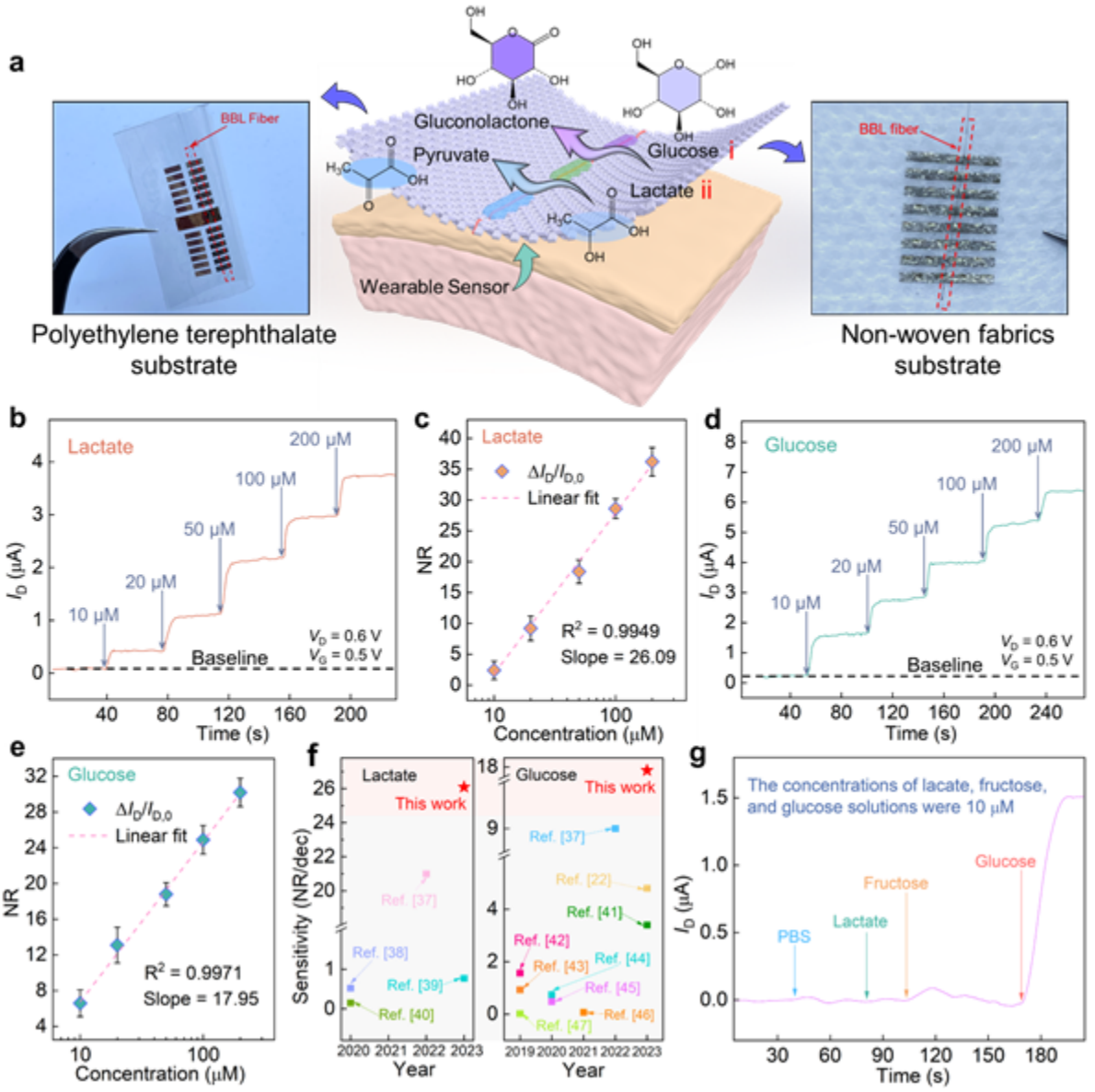

Figure 4. Schematic illustration and performance comparison of the BBL fiber OECT-based sensors. a) BBL fiber OECT-based sensors with different substrates and the schematic diagram of the wearable sensors for lactate and glucose sensing. Real-time I_D response of the $BBL_{60,38}$ fiber OECT-based sensors as successive amounts of lactate/PBS and glucose/PBS solutions were added to the gate electrodes containing **b)** lactate oxidase (LOx) and **d)**

glucose oxidase (GOx). Normalized response (NR) curves derived from the chronoamperometric response of the $BBL_{60,38}$ fiber OECT-based **c)** lactate and **e)** glucose sensors. **f)** Sensitivity comparison of BBL fiber OECT-based sensors and other reported sensors for lactate[37-40] and glucose[23,37,41-47] sensing. **g)** Real-time I_D response of the BBL fiber OECT-based sensor as adding glucose and non-relevant biomolecules including PBS, lactate, and fructose solutions. The amount of each addition was 10 μL, and the concentration of lactate, fructose, and glucose solutions was 10 μM.

To date, complementary logic circuits have rarely been demonstrated for fiber-based OECTs, largely due to the unbalanced n- and p-type fiber OECT performance and stability.[48] We fabricated a complementary accumulation-mode inverter by combining a p-type $P(lgDPP\text{-}MeOT2)_{60,38}$ fiber and an n-type $BBL_{60,38}$ fiber (**Figure 5**a). The voltage output characteristics shown in Figure 5b indicated that the fiber inverter showed a sharp voltage transition with a gain of approximately 38 V V^{-1} at V_{DD} = 0.7 V (Figure 5c), which is among the highest values in complementary-type OECT inverters. In addition, the maximum static power consumption (P_{max}) was only 2.64 μW (Figure 5d). The realization of the fiber inverters will facilitate the integration of these fiber OECT devices and technologies into a wider range of complementary-type electronics.

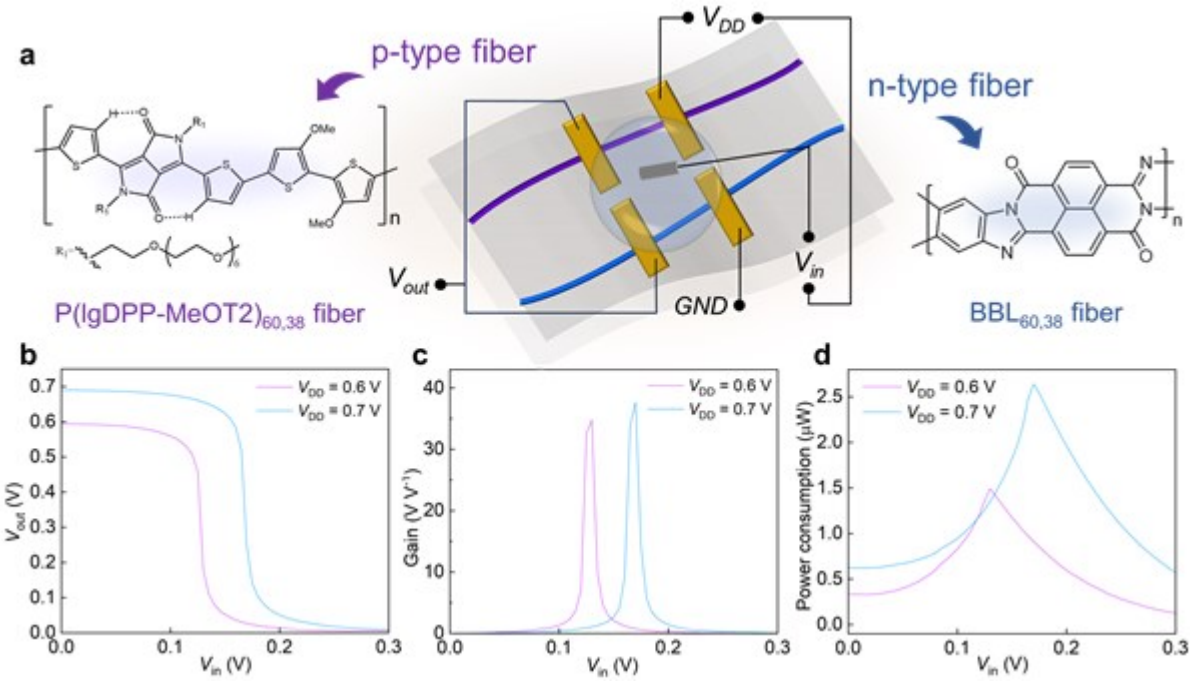

Figure 5. Fiber-based complementary inverters and their performance. a) Schematic of the complementary-type inverter and chemical structures of p-type P(lgDPP-MeOT2) and n-type BBL polymers. **b)** Voltage transfer characteristics, **c)** voltage gains, and **d)** power consumptions of the fiber-based inverter at different supply voltages. The supply voltage (V_{DD}) is 0.6 V or 0.7 V.

3. Conclusions

In summary, we have successfully produced high-performance BBL fibers with enhanced stability using a simple wet-spinning approach. The rapid removal of BBL solvent (MSA) during spinning allows for adjustable fiber diameters. The BBL fiber OECTs exhibit a high area-normalized transconductance ($g_{m,A}$) of 2.40 μS μm^{-2} and unprecedented high

stability, largely due to their closer π-π stacking, better chain alignment, and stronger interchain interactions. The high-performance and ultra-stable BBL fiber OECTs can not only work as biosensors with high sensitivity and good selectivity but also enable the construction of fiber-based complementary inverters with high gains. Our work demonstrates a promising fabrication technology for high-performance and stable OECTs and opens a wider palette for fiber-based bioelectronics.

Supporting Information

Supporting Information is available from the Wiley Online Library or from the author.

Acknowledgments

This work is supported by the National Natural Science Foundation of China (92156019 and 22075001) and the National Key R&D Program of China (2022YFE0130600). The computational part is supported by the High-Performance Computing Platform of Peking University. We acknowledge the Molecular Materials and Nanofabrication Laboratory (MMNL) in the College of Chemistry and Electron Microscopy Laboratory of Peking University for the use of instruments. We thank beamline BL14B1 (Shanghai Synchrotron Radiation Facility) for providing beamtime for part of the XRD study.

Conflict of Interest

The authors declare no conflict of interest.

Data Availability Statement

The data that support the findings of this study are available from the corresponding author upon reasonable request.

References

[1] S. Yuvaraja, A. Nawaz, Q. Liu, D. Dubal, S. G. Surya, K. N. Salama, P. Sonar, *Chem. Soc. Rev.* **2020**, *49*, 3423.

[2] M. Y. Lee, H. R. Lee, C. H. Park, S. G. Han, J. H. Oh, *Acc. Chem. Res.* **2018**, *51*, 2829.

[3] C. Cea, G. D. Spyropoulos, P. Jastrzebska-Perfect, J. J. Ferrero, J. N. Gelinas, D. Khodagholy, *Nat. Mater.* **2020**, *19*, 679.

[4] P. R. Paudel, V. Kaphle, D. Dahal, R. K. Radha Krishnan, B. Lüssem, *Adv. Funct. Mater.* **2021**, *31*, 2004939.

[5] D. Khodagholy, J. Rivnay, M. Sessolo, M. Gurfinkel, P. Leleux, L. H. Jimison, E. Stavrinidou, T. Herve, S. Sanaur, R. M. Owens, G. G. Malliaras, *Nat. Commun.* **2013**, *4*, 2133.

[6] J. Rivnay, S. Inal, A. Salleo, R. M. Owens, M. Berggren, G. G. Malliaras, *Nat. Rev. Mater.* **2018**, *3*, 17086.

[7] Y. Liang, F. Brings, V. Maybeck, S. Ingebrandt, B. Wolfrum, A. Pich, A. Offenhäusser, D. Mayer, *Adv. Funct. Mater.* **2019**, *29*, 1902085.

[8] F. Bonafè, F. Decataldo, I. Zironi, D. Remondini, T. Cramer, B. Fraboni, *Nat. Commun.* **2022**, *13*, 5423.

[9] M. Ghittorelli, L. Lingstedt, P. Romele, N. I. Crăciun, Z. M. Kovács-Vajna, P. W. M. Blom, F. Torricelli, *Nat. Commun.* **2018**, *9*, 1441.

[10] G. A. Woods, N. J. Rommelfanger, G. Hong, *Matter* **2020**, *3*, 1087.

[11] G. Rong, S. R. Corrie, H. A. Clark, *ACS Sens.* **2017**, *2*, 327.

[12] A. M. Nightingale, C. L. Leong, R. A. Burnish, S.-u. Hassan, Y. Zhang, G. F. Clough, M. G. Boutelle, D. Voegeli, X. Niu, *Nat. Commun.* **2019**, *10*, 2741.

[13] E. Musk, *J. Medical Internet Res.* **2019**, *21*, e16194.

[14] W. Huang, J. Chen, Y. Yao, D. Zheng, X. Ji, L.-W. Feng, D. Moore, N. R. Glavin, M. Xie, Y. Chen, R. M. Pankow, A. Surendran, Z. Wang, Y. Xia, L. Bai, J. Rivnay, J. Ping, X. Guo, Y. Cheng, T. J. Marks, A. Facchetti, *Nature* **2023**, *613*, 496.

[15] N. Li, Y. Li, Z. Cheng, Y. Liu, Y. Dai, S. Kang, S. Li, N. Shan, S. Wai, A. Ziaja, Y. Wang, J. Strzalka, W. Liu, C. Zhang, X. Gu, J. A. Hubbell, B. Tian, S. Wang, *Science* **2023**, *381*, 686.

[16] C. Cea, Z. Zhao, D. J. Wisniewski, G. D. Spyropoulos, A. Polyravas, J. N. Gelinas, D. Khodagholy, *Nat. Mater.* **2023**, *22*, 1227.

[17] Y. Lei, P. Li, Y. Zheng, T. Lei, *Mater. Chem. Front.* **2024**, *8*, 133.

[18] H. Sun, J. Gerasimov, M. Berggren, S. Fabiano, *J. Mater. Chem. C* **2018**, *6*, 11778.

[19] S. Chen, A. Surendran, X. Wu, S. Y. Lee, M. Stephen, W. L. Leong, *Adv. Mater. Technol.* **2020**, *5*, 2000523.

[20] A. Giovannitti, C. B. Nielsen, D.-T. Sbircea, S. Inal, M. Donahue, M. R. Niazi, D. A. Hanifi, A. Amassian, G. G. Malliaras, J. Rivnay, I. McCulloch, *Nat. Commun.* **2016**, *7*, 13066.

[21] P. Li, J. Shi, Y. Lei, Z. Huang, T. Lei, *Nat. Commun.* **2022**, *13*, 5970.

[22] Y. Wang, E. Zeglio, H. Liao, J. Xu, F. Liu, Z. Li, I. P. Maria, D. Mawad, A. Herland, I. McCulloch, W. Yue, *Chem. Mater.* **2019**, *31*, 9797.

[23] W. Wu, K. Feng, Y. Wang, J. Wang, E. Huang, Y. Li, S. Y. Jeong, H. Y. Woo, K. Yang, X. Guo, *Adv. Mater.* **2024**, *36*, 2310503.

[24] H. Sun, M. Vagin, S. Wang, X. Crispin, R. Forchheimer, M. Berggren, S. Fabiano, *Adv. Mater.* **2018**, *30*, 1704916.

[25] A. Babel, S. A. Jenekhe, *J. Am. Chem. Soc.* **2003**, *125*, 13656.

[26] J. Wu, X. Rui, C. Wang, W.-B. Pei, R. Lau, Q. Yan, Q. Zhang, *Adv. Energy Mater.* **2015**, *5*, 1402189.

[27] J. Rivnay, S. C. B. Mannsfeld, C. E. Miller, A. Salleo, M. F. Toney, *Chem. Rev.* **2012**, *112*, 5488.

[28] A. M. Hindeleh, R. Hosemann, *J. Phys. C: Solid State Phys.* **1988**, *21*, 4155.

[29] M. Ponçot, J. Martin, S. Chaudemanche, O. Ferry, T. Schenk, J. P. Tinnes, D. Chapron, I. Royaud, A. Dahoun, P. Bourson, *Polymer* **2015**, *80*, 27.

[30] H. Y. Wu, C. Y. Yang, Q. Li, N. B. Kolhe, X. Strakosas, M. A. Stoeckel, Z. Wu, W. Jin, M. Savvakis, R. Kroon, D. Tu, H. Y. Woo, M. Berggren, S. A. Jenekhe, S. Fabiano, *Adv. Mater.* **2022**, *34*, 2106235.

[31] X. Tang, H. Shen, S. Zhao, N. Li, J. Liu, *Nat. Electron.* **2023**, *6*, 109.

[32] S. Zhang, M. U. Ocheje, L. Huang, L. Galuska, Z. Cao, S. Luo, Y. H. Cheng, D. Ehlenberg, R. B. Goodman, D. Zhou, Y. Liu, Y. C. Chiu, J. D. Azoulay, S. Rondeau-Gagné, X. Gu, *Adv. Electron. Mater.* **2019**, *5*, 1800899.

[33] A. X. Chen, A. T. Kleinschmidt, K. Choudhary, D. J. Lipomi, *Chem. Mater.* **2020**, *32*, 7582.

[34] S. E. Root, S. Savagatrup, A. D. Printz, D. Rodriquez, D. J. Lipomi, *Chem. Rev.* **2017**, *117*, 6467.

[35] Z. Wei, X. Wang, B. Seo, X. Luo, Q. Hu, J. Jones, M. Zeller, K. Wang, B. M. Savoie, K. Zhao, L. Dou, *Angew. Chem. Int. Ed.* **2022**, *61*, e202213840.

[36] M. Xie, H. Liu, M. Wu, C. Chen, J. Wen, L. Bai, J. Yu, W. Huang, *Org. Electron.* **2023**, *117*, 106777.

[37] S. Demuru, C.-H. Huang, K. Parvez, R. Worsley, G. Mattana, B. Piro, V. Noël, C. Casiraghi, D. Briand, *ACS Appl. Nano Mater.* **2022**, *5*, 1664.

[38] Q. Zhang, D. Jiang, C. Xu, Y. Ge, X. Liu, Q. Wei, L. Huang, X. Ren, C. Wang, Y. Wang, *Sens. Actuators B* **2020**, *320*, 128325.

[39] S. Baek, H. Matsui, T. Mano, J. A. Park, Y. Jo, Y. Lee, S. Tokito, J. Kwon, S. Jung, *Biosens. Bioelectron.* **2023**, *222*, 114958.

[40] Y. Zhang, Y. Wang, X. Qing, Y. Wang, W. Zhong, W. Wang, Y. Chen, Q. Liu, M. Li, D. Wang, *Anal. Bioanal. Chem.* **2020**, *412*, 7515.

[41] N. Fumeaux, C. P. Almeida, S. Demuru, D. Briand, *Sci. Rep.* **2023**, *13*, 11467.

[42] Y. Cui, F. Chen, X.-B. Yin, *Biosens. Bioelectron.* **2019**, *135*, 208.

[43] A. Savva, D. Ohayon, J. Surgailis, A. F. Paterson, T. C. Hidalgo, X. Chen, I. P. Maria, B. D. Paulsen, A. J. Petty, J. Rivnay, I. McCulloch, S. Inal, *Adv. Electron. Mater.* **2019**, *5*, 1900249.

[44] D. Ohayon, G. Nikiforidis, A. Savva, A. Giugni, S. Wustoni, T. Palanisamy, X. Chen, I. P. Maria, E. Di Fabrizio, P. M. F. J. Costa, I. McCulloch, S. Inal, *Nat. Mater.* **2020**, *19*, 456.

[45] C. Diacci, J. W. Lee, P. Janson, G. Dufil, G. Méhes, M. Berggren, D. T. Simon, E. Stavrinidou, *Adv, Mater. Technol.* **2020**, *5*, 1900262.

[46] J. Fan, A. A. Forero Pico, M. Gupta, *Mater. Adv.* **2021**, *2*, 7445.

[47] M. Li, H. Wang, X. Wang, Q. Lu, H. Li, Y. Zhang, S. Yao, *Biosens. Bioelectron.* **2019**, *142*, 111535.

[48] X. Wu, T. L. D. Tam, S. Chen, T. Salim, X. Zhao, Z. Zhou, M. Lin, J. Xu, Y. L. Loo, W. L. Leong, *Adv. Mater.* **2022**, *34*, 2206118.A meticulously designed wet-spinning method successfully produces n-type semiconducting fibers with reduced π-π stacking distance and

ordered molecular arrangement. Organic electrochemical transistors (OECTs) based on these fibers exhibit superior performance and unprecedented stability, advancing the development of highly sensitive biosensors and fiber-based complementary logic circuits, and paving the way for fiber-based bioelectronics.

Xiu Wang, Zhi Zhang,* Peiyun Li, Jingcao Xu, Yuting Zheng, Wenxi Sun, Mingyue Xie, Juanrong Wang, Xiran Pan, Xun Lei, Jingyi Wang, Jupeng Chen, Yiheng Chen, Shu-Jen Wang, Ting Lei*

Ultra-Stable N-Type Semiconducting Fiber Organic Electrochemical Transistors for Highly Sensitive Biosensors